Magnetic field effects in electron systems with imperfect nesting

A. O. Sboychakov,[1] A. L. Rakhmanov,[1,2,3] K. I. Kugel,[1,4] A. V. Rozhkov,[1,3] and Franco Nori[5,6]
[1]*Institute for Theoretical and Applied Electrodynamics, Russian Academy of Sciences, Moscow 125412, Russia*
[2]*Dukhov Research Institute of Automatics, Moscow 127055, Russia*
[3]*Moscow Institute for Physics and Technology (State University), Moscow region 141700, Russia*
[4]*National Research University Higher School of Economics, Moscow 109028, Russia*
[5]*Center for Emergent Matter Science, RIKEN, Wako-shi, Saitama, 351-0198, Japan*
[6]*Department of Physics, University of Michigan, Ann Arbor, Michigan 48109-1040, USA*
(Received 21 September 2016; published 5 January 2017)

We analyze the effects of an applied magnetic field on the phase diagram of a weakly correlated electron system with imperfect nesting. The Hamiltonian under study describes two bands: electron and hole ones. Both bands have spherical Fermi surfaces, whose radii are slightly mismatched due to doping. These types of models are often used in the analysis of magnetic states in chromium and its alloys, superconducting iron pnictides, AA-type bilayer graphene, borides, etc. At zero magnetic field, the uniform ground state of the system turns out to be unstable against electronic phase separation. The applied magnetic field affects the phase diagram in several ways. In particular, the Zeeman term stabilizes new antiferromagnetic phases. It also significantly shifts the boundaries of inhomogeneous (phase-separated) states. At sufficiently high fields, the Landau quantization gives rise to oscillations of the order parameters and of the Néel temperature as a function of the magnetic field.

DOI: 10.1103/PhysRevB.95.014203

I. INTRODUCTION

Fermi surface nesting is a very popular and important concept in condensed matter physics [1]. The existence of two fragments of the Fermi surface, which can be matched upon translation by a certain reciprocal lattice vector (nesting vector), entails an instability of a Fermi-liquid state. A superstructure or additional order parameter related to nesting vector is generated due to the instability. The nesting is widely invoked for the analysis of charge density wave (CDW) states [2,3], spin density waves (SDW) states [4,5], mechanisms of high-T_c superconductivity [6–8], fluctuating charge/orbital modulation in magnetic oxides [9], chromium and its alloys [10–13], etc.

It is important to emphasize that in a real material the nesting may be imperfect, i.e., the Fermi surface fragments can only match approximately. One of the earliest studies of imperfect nesting was performed by Rice [13] in the context of chromium and its alloys (see also the review articles Refs. [14,15]).

The notion of nesting and related concepts were broadly employed in the recent studies of iron-based pnictides [16–22]. For example, Ref. [16] argued that the deviation from the perfect nesting lifts degeneracy between several competing magnetically ordered states. The influence of the imperfect nesting on the phase coexistence was discussed in Ref. [19].

Many theoretical investigations assume from the outset the homogeneity of the electron state. This assumption may be violated in systems with imperfect nesting. Indeed, it was demonstrated that the imperfect-nesting mechanism can be responsible for the nanoscale phase separation in quasi-one-dimensional metals [23], chromium alloys [24], iron-based superconductors [25], and in doped bilayer graphene [26–28]. Several experiments on pnictides [29–35] and chalcogenides [36–38] support the possibility of phase separation (see also review article [39]).

In similar context of imperfect nesting, studies of spin and charge inhomogeneities are currently active in the physics of low-dimensional compounds [40–42]. Other types of inhomogeneous states ("stripes," domain walls, impurity levels) were also discussed in the literature in the framework of analogous models [23,43,44]. Moreover, it was shown that the possibility of SDW ordering in systems with itinerant charge carriers results in very rich and complicated phase diagrams involving phase-separation regions [45,46].

An applied magnetic field **B** alters the quasiparticle states, changing the nesting conditions. In the present paper, we explore the physical consequences of the applied magnetic field for weakly correlated electron systems with imperfect nesting. In a generic situation, the magnetic field enters the Hamiltonian both via the Zeeman term, and via the substitution $\hat{\mathbf{p}} \to \hat{\mathbf{p}} + (e/c)\mathbf{A}$. The Zeeman term lifts the degeneracy with respect to the spin projection. Both electron and hole Fermi surface sheets become split into two spin-polarized components. As a result, two different SDW order parameters corresponding to spin projections parallel and antiparallel to the direction of **B** can be constructed. When the electron-hole symmetry between the electron and hole pockets is absent, the effects of the Zeeman term is especially pronounced. In particular, new antiferromagnetic (AFM) phases, both homogeneous and inhomogeneous, appear in the phase diagram. The boundaries between different phases exhibit strong dependence on B. For example, such effects were found in the analysis of the magnetic phase diagram of doped rare-earth borides [47].

We also study separately phenomena caused by the Landau quantization. In the range of high magnetic fields, Landau quantization leads to characteristic oscillations of the SDW order parameters and of the Néel temperature as a function of B. However, these oscillations are most clearly pronounced in the case of symmetric electron and hole pockets. Otherwise, the nesting and, hence, the SDW ordering would be completely destroyed by the magnetic field before any detectable oscillations would occur. Similar oscillatory effects are well-known in the context of quasi-one-dimensional compounds [48–53].

However, the role of the magnetic field in nesting-related phenomena in the usual three-dimensional materials has received only limited attention [11,54].

This paper is organized as follows. In Sec. II, we formulate the model. Section III deals with the effects related to the Zeeman term. Phenomena occurring due to the Landau quantization are treated in Sec. IV. A discussion of the results is given in Sec. V. Some details of the calculations are presented in Appendix.

II. MODEL

A. Hamiltonian

The model under study is schematically illustrated in Fig. 1. It describes two bands: an electronic band (a) and a hole band (b). The hole Fermi surface coincides with the electron Fermi surface after a translation by a reciprocal lattice vector $\mathbf{Q}_0$. The quasiparticles interact with each other via a short-range repulsive potential. Formally, the Hamiltonian is represented as

$$\hat{H} = \hat{H}_e + \hat{H}_{\rm int}, \tag{1}$$

where $\hat{H}_e$ is the single-electron term, and $\hat{H}_{\rm int}$ corresponds to the interaction between quasiparticles.

Regarding the single-electron term, we assume a quadratic dispersion for both bands and use the Wigner-Seitz approximation. Specifically, in the electron band, the wave vector $\mathbf{k}$ is confined within a sphere of finite radius centered around zero, and in the hole band, such sphere is centered at $\mathbf{Q}_0$. The kinetic energies of these states are spread between the minimum values (denoted by $\varepsilon^{a,b}_{\rm min}$) and maximum values $\varepsilon^{a,b}_{\rm max}$, see Fig. 1. Thus, the energy spectra for the electron and hole pockets, measured relative to the Fermi energy μ, have the

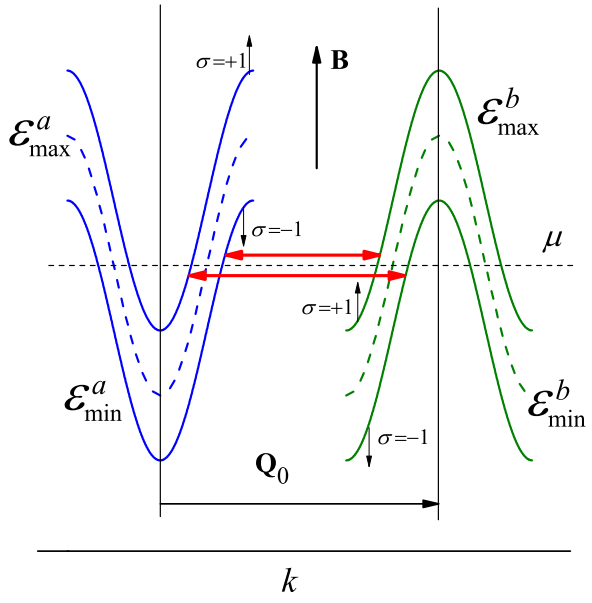

FIG. 1. Band structure of the electron model in an applied magnetic field. The magnetic field lifts the degeneracy of the electron-like (a) and hole-like (b) bands with respect to the electron spin. The red arrows indicate the interband coupling giving rise to the order parameters. The splitting into Landau levels is not shown.

form ($\hbar = 1$)

$$\varepsilon^a(\mathbf{k}) = \frac{\mathbf{k}^2}{2m_a} + \varepsilon^a_{\rm min} - \mu, \quad \varepsilon^a_{\rm min} < \varepsilon^a < \varepsilon^a_{\rm max},$$
$$\varepsilon^b(\mathbf{k}+\mathbf{Q}_0) = -\frac{\mathbf{k}^2}{2m_b} + \varepsilon^b_{\rm max} - \mu, \quad \varepsilon^b_{\rm min} < \varepsilon^b < \varepsilon^b_{\rm max}. \tag{2}$$

The nesting conditions mean that for some $\mu = \mu_0$, the Fermi surfaces of the a and b bands coincide after a translation by the vector $\mathbf{Q}_0$, and both Fermi spheres are characterized by the single Fermi momentum k_F. Using Eq. (2), we readily obtain

$$k_F^2 = \frac{2m_a m_b}{m_a + m_b}\left(\varepsilon^b_{\rm max} - \varepsilon^a_{\rm min}\right), \quad \mu_0 = \frac{m_b \varepsilon^b_{\rm max} + m_a \varepsilon^a_{\rm min}}{m_a + m_b}. \tag{3}$$

Below, we will measure the momentum of the b band from the nesting vector $\mathbf{Q}_0$, that is, we replace $\varepsilon^b(\mathbf{k}+\mathbf{Q}_0) \to \varepsilon^b(\mathbf{k})$ in Eq. (2). For perfect electron-hole symmetry, when $m_a = m_b = m$ and $\varepsilon^b_{\rm max} = -\varepsilon^a_{\rm min}$, we obtain $\mu_0 = 0$.

In an applied uniform dc magnetic field $\mathbf{B}$, the single-electron part of our model can be written as

$$\hat{H}_e = \sum_{\alpha\sigma} \int d^3x\, \psi^\dagger_{\alpha\sigma}(\mathbf{x}) \hat{H}_{\alpha\sigma} \psi_{\alpha\sigma}(\mathbf{x}), \tag{4}$$

where [see Eq. (2)]

$$\hat{H}_{a\sigma} = \frac{\left(\hat{\mathbf{p}} + \frac{e}{c}\mathbf{A}\right)^2}{2m_a} + \sigma g_a \omega_a + \varepsilon^a_{\rm min} - \mu,$$
$$\hat{H}_{b\sigma} = -\frac{\left(\hat{\mathbf{p}} + \frac{e}{c}\mathbf{A}\right)^2}{2m_b} + \sigma g_b \omega_b + \varepsilon^b_{\rm max} - \mu. \tag{5}$$

In these equations, $\alpha = a,b$, $\hat{\mathbf{p}} = -i\nabla$ is the momentum operator, $\sigma = \pm 1$ is the spin projection, $\omega_\alpha = eB/cm_\alpha$ are the cyclotron frequencies for the electron and hole bands, and g_α are the corresponding Landé factors. We assume that the magnetic field is directed along the z axis and choose the Landau gauge for the vector potential, $\mathbf{A} = (-By,0,0)$.

The second term in Eq. (1) describes the interaction between electrons and holes. For treating the SDW instability, it is sufficient to keep only the interaction between the a and b bands. The neglected intraband contributions can only renormalize the parameters. We also assume that this interaction is a short-range one. Thus, we can write

$$\hat{H}_{\rm int} = V \sum_{\sigma\sigma'} \int d^3x\, \psi^\dagger_{a\sigma}(\mathbf{x}) \psi_{a\sigma}(\mathbf{x}) \psi^\dagger_{b\sigma'}(\mathbf{x}) \psi_{b\sigma'}(\mathbf{x}). \tag{6}$$

The coupling constant V is positive, which corresponds to repulsion.

B. Single-electron spectrum in a magnetic field

Let us start with a brief discussion of the properties of the single-electron Hamiltonian. When the magnetic field is zero, the single-electron spectrum consists of two bands of free fermions with two-fold spin degeneracy. In a nonzero applied magnetic field $\mathbf{B}$, the operator $\psi_{\alpha\sigma}(\mathbf{x})$ can be expressed as a series expansion in terms of eigenfunctions of Hamiltonian (4),

$$\psi_{\alpha\sigma}(\mathbf{x}) = \sum_{\mathbf{p}n} \frac{e^{i(p_x x + p_z z)}}{\sqrt{\mathcal{V}^{2/3} l_B}} \chi_n\left(\frac{y - p_x l_B^2}{l_B}\right) \psi_{\mathbf{p}n\alpha\sigma}, \tag{7}$$

where $\psi_{\mathbf{p}n\alpha\sigma}$ is the annihilation operator for an electron in band α with 2D momentum $\mathbf{p} = (p_x, p_z)$ and spin projection σ at the Landau level n, symbol $\mathcal{V}$ denotes the system volume, $l_B = \sqrt{c/eB}$ is the magnetic length,

$$\chi_n(\xi) = \frac{1}{\sqrt{2^n n!\sqrt{\pi}}} e^{-\xi^2/2} H_n(\xi), \tag{8}$$

and $H_n(\xi)$ is the Hermite polynomial of degree n. In this basis, the Hamiltonian can be expressed as

$$\hat{H}_e = \sum_{\mathbf{p}n\alpha\sigma} \varepsilon_{\alpha\sigma}(p_z,n) \psi^\dagger_{\mathbf{p}n\alpha\sigma} \psi_{\mathbf{p}n\alpha\sigma}, \tag{9}$$

where the single-particle eigenenergies are

$$\begin{aligned} \varepsilon^a_\sigma(p_z,n) &= \omega_a\left(n + \frac{1}{2} + \sigma g_a\right) + \frac{p_z^2}{2m_a} + \varepsilon^a_{\min} - \mu, \\ \varepsilon^b_\sigma(p_z,n) &= -\omega_b\left(n + \frac{1}{2} - \sigma g_b\right) - \frac{p_z^2}{2m_b} + \varepsilon^b_{\max} - \mu. \end{aligned} \tag{10}$$

The spectrum consists of four bands (see Fig. 1) since the Zeeman term (the term, proportional to σ) lifts the degeneracy with respect to the electron spin.

C. Energy scales

The energy spectrum of the model is characterized by two single-particle energy scales. The first is the Fermi energy $\varepsilon_{F\alpha} = k_F^2/2m_\alpha$, and the second is ω_α, which is the distance between the Landau levels in band α. Furthermore, we assume that $\varepsilon_{Fa} \approx \varepsilon_{Fb}$ and $\omega_a \approx \omega_b$. The energy scale associated with the interactions will be characterized by the value of a spectral gap Δ_0. The latter parameter is defined as follows. When $\mu \approx \mu_0$, the nesting between the two sheets of the Fermi surface is nearly perfect. It is known that, under such condition, the interaction between the electron- and hole-like bands opens a gap $\Delta(T,B)$ in the electron spectrum. The value of the gap at zero temperature $T = 0$ and zero magnetic field $B = 0$ will be denoted as $\Delta_0 = \Delta(0,0)$.

Below we consider the case $\Delta_0 \ll \varepsilon_{F\alpha}$, which corresponds to a weak electron-hole coupling. We also classify the magnetic field as low if $\omega_\alpha \lesssim \Delta_0$, and high if $\omega_\alpha \gtrsim \Delta_0$. The Landau quantization is of importance in the high-field range, whereas at low fields, it can be neglected. In the regime of low magnetic fields considered in the next Sec. III, we neglect any corrections associated with the small ratio $\omega_\alpha/\varepsilon_{F\alpha}$, while for $\omega_\alpha \gtrsim \Delta_0$ (this regime is considered in Sec. IV), we take into account these corrections in the leading order, which turns out to be of the order of $(\omega_\alpha/\varepsilon_{F\alpha})^{1/2}$.

III. ELECTRON-HOLE COUPLING: LOW MAGNETIC FIELD

A. Main definitions

At low magnetic fields, we can neglect the effect of the Landau quantization on the electron spectrum and take into account only the Zeeman splitting. In this approximation, the single-electron Hamiltonian (9) has the form

$$\hat{H}_e = \sum_{\mathbf{k}\alpha\sigma} \varepsilon_{\alpha\sigma}(\mathbf{k}) \psi^\dagger_{\mathbf{k}\alpha\sigma} \psi_{\mathbf{k}\alpha\sigma}, \tag{11}$$

where $\psi^\dagger_{\mathbf{k}\alpha\sigma}$ and $\psi_{\mathbf{k}\alpha\sigma}$ are the creation and annihilation operators of an electron in band α with (3D) momentum $\mathbf{k}$ and spin projection σ, while the electron spectra now read

$$\begin{aligned} \varepsilon^a_\sigma(\mathbf{k}) &= \frac{k^2 - k_F^2}{2m_a} + \sigma g_a \omega_a - \delta\mu, \\ \varepsilon^b_\sigma(\mathbf{k}) &= -\frac{k^2 - k_F^2}{2m_b} + \sigma g_b \omega_b - \delta\mu, \end{aligned} \tag{12}$$

where $\delta\mu = \mu - \mu_0$.

If the applied magnetic field is zero, the commensurate SDW order parameter can be written as

$$\Delta = \frac{V}{\mathcal{V}} \sum_{\mathbf{k}} \langle \psi^\dagger_{\mathbf{k}a\sigma} \psi_{\mathbf{k}b\bar{\sigma}} \rangle, \tag{13}$$

where $\bar{\sigma}$ means $-\sigma$. This order parameter is degenerate with respect to spin. If $\mathbf{B} \neq 0$, this degeneracy is lifted and we introduce a two-component order parameter corresponding to the nesting vectors shown by the arrows in Fig. 1,

$$\Delta_\uparrow = \frac{V}{\mathcal{V}} \sum_{\mathbf{k}} \langle \psi^\dagger_{\mathbf{k}a\uparrow} \psi_{\mathbf{k}b\downarrow} \rangle, \quad \Delta_\downarrow = \frac{V}{\mathcal{V}} \sum_{\mathbf{k}} \langle \psi^\dagger_{\mathbf{k}a\downarrow} \psi_{\mathbf{k}b\uparrow} \rangle. \tag{14}$$

The mean-field spectrum of the model has a form

$$E^\sigma_{1,2}(\mathbf{k}) = \frac{\varepsilon^a_\sigma(\mathbf{k}) + \varepsilon^b_{-\sigma}(\mathbf{k})}{2} \pm \sqrt{\Delta_\sigma^2 + \left(\frac{\varepsilon^a_\sigma(\mathbf{k}) - \varepsilon^b_{-\sigma}(\mathbf{k})}{2}\right)^2}. \tag{15}$$

Using these spectra, we can write the grand potential of the system in the mean-field approximation as a sum of two "decoupled" terms $\Omega = \Omega_\uparrow + \Omega_\downarrow$, where "partial" grand potentials are equal to

$$\Omega_\sigma = \mathcal{V}\left[\frac{\Delta_\sigma^2}{V} - T \sum_{s=1,2} \int \frac{d^3\mathbf{k}}{(2\pi)^3} \ln(1 + e^{-E^\sigma_s(\mathbf{k})/T})\right]. \tag{16}$$

The order parameters are found by minimizing Ω with respect to Δ_σ.

B. SDW order parameters

The case when the electron and hole bands are perfectly symmetric is, of course, the simplest. In such a situation, however, the effect of weak magnetic fields on the electron spectrum is zero, as it will be evident below. Thus, we should introduce some electron-hole asymmetry to obtain nontrivial results in the low-field range. Qualitatively, a particular source of the asymmetry is not of importance. Here, we assume for simplicity that $m_a = m_b = m$ (hence, $\omega_a = \omega_b = \omega_H$ and $\varepsilon_{Fa} = \varepsilon_{Fb} = \varepsilon_F$), but $g_a \neq g_b$. It is also assumed that the difference $g_a - g_b$ is of the same order as g_a and g_b.

We rewrite Eq. (12) in the following convenient form:

$$\begin{aligned} \varepsilon^a_\sigma(\mathbf{k}) &= \left(\frac{k^2}{2m} - E_{F\sigma}\right) - \mu_\sigma, \\ \varepsilon^b_{-\sigma}(\mathbf{k}) &= -\left(\frac{k^2}{2m} - E_{F\sigma}\right) - \mu_\sigma, \end{aligned} \tag{17}$$

where the following notation is used:

$$g = \frac{g_a + g_b}{2}, \quad \Delta g = \frac{g_a - g_b}{2},$$
$$E_{F\sigma} = \frac{k_F^2}{2m} - \sigma g \omega_H, \quad \mu_\sigma = \delta\mu - \sigma \Delta g \omega_H. \tag{18}$$

As we stated above, in the low-field range, we neglect corrections of the order of ω_H/E_F, since $\omega_H \ll \Delta_0 \ll E_F$. Then, we take into account only terms of the order of ω_H/Δ_0. Expanding the spectra in Eq. (17) near the Fermi momentum, we obtain

$$\varepsilon_\sigma^a(\mathbf{k}) \approx v_F \delta k + \sigma g \omega_H - \mu_\sigma, \tag{19}$$
$$\varepsilon_{-\sigma}^b(\mathbf{k}) \approx -v_F \delta k - \sigma g \omega_H - \mu_\sigma,$$

where $\delta k = |\mathbf{k}| - k_F$ and $v_F = k_F/m$.

Substituting Eqs (19) in Eqs. (15) and (16) and performing integration, we obtain the expression for grand potential

$$\frac{\Omega}{\mathcal{V}} = 2N_F \sum_\sigma \Bigg[-\frac{\Delta_\sigma^2}{2}\left(\ln\frac{\Delta_0}{\Delta_\sigma} + \frac{1}{2}\right) + \int_0^\infty d\xi \ln\Big[f_F\Big(\sqrt{\Delta_\sigma^2 + \xi^2} - \mu_\sigma\Big) \times f_F\Big(\sqrt{\Delta_\sigma^2 + \xi^2} + \mu_\sigma\Big)\Big]\Bigg], \tag{20}$$

where $f_F(\epsilon) = 1/[1 + \exp(\epsilon/T)]$ is the Fermi function, and Δ_0 is the SDW gap at zero field, temperature, and doping ($\mu = \mu_0$)

$$\Delta_0 \approx \varepsilon_F \exp(-1/VN_F), \quad N_F = \frac{k_F^2}{2\pi^2 v_F}. \tag{21}$$

From the minimization conditions $\partial\Omega/\partial\Delta_\sigma = 0$, we derive equations for the order parameters:

$$\ln\frac{\Delta_0}{\Delta_\sigma} = \int_0^\infty d\xi \frac{f_F\Big(\sqrt{\Delta_\sigma^2+\xi^2}+\mu_\sigma\Big) + f_F\Big(\sqrt{\Delta_\sigma^2+\xi^2}-\mu_\sigma\Big)}{\sqrt{\Delta_\sigma^2 + \xi^2}}. \tag{22}$$

The electron density is

$$N = \frac{1}{\mathcal{V}} \sum_{\mathbf{k}s\sigma} f_F\big[E_s^\sigma(\mathbf{k})\big]. \tag{23}$$

The parameter N_0 corresponds to the ideal nesting, $\delta\mu = 0$, in the absence of the magnetic field, $B = 0$. We define the doping level as $X = N - N_0$. The equation for X can be written in the form

$$\frac{X}{N_F} = \sum_\sigma \int_0^\infty d\xi \big[f_F(\sqrt{\Delta_\sigma^2 + \xi^2} - \mu_\sigma) - f_F\Big(\sqrt{\Delta_\sigma^2+\xi^2}+\mu_\sigma\Big)\big]. \tag{24}$$

The derivation of this equation is straightforward (the details can be found in Ref. [24]). The value of X can also be considered as a shift from the position of ideal nesting. In our terms, "zero doping" really means "perfect nesting."

For further calculations, it is convenient to introduce the following dimensionless variables:

$$x = \frac{X}{N_F\Delta_0}, \ \nu = \frac{\delta\mu}{\Delta_0}, \ b = \frac{\Delta g \omega_H}{\Delta_0}, \ \delta_\sigma = \frac{\Delta_\sigma}{\Delta_0}. \tag{25}$$

In this notation, we rewrite Eqs. (22) and (24) as

$$\ln\frac{1}{\delta_\sigma} = \int_0^\infty \frac{d\xi}{\eta_\sigma}[f_F(\eta_\sigma + \nu - \sigma b) + f_F(\eta_\sigma - \nu + \sigma b)],$$
$$x = \int_0^\infty d\xi \sum_\sigma [f_F(\eta_\sigma - \nu + \sigma b) - f_F(\eta_\sigma + \nu - \sigma b)], \tag{26}$$

where $\eta_\sigma = \sqrt{\delta_\sigma^2 + \xi^2}$. We also introduce the dimensionless grand potential

$$\varphi = \frac{\pi^2 v_F}{k_F^2 \Delta_0^2}\frac{\Omega}{\mathcal{V}}. \tag{27}$$

Using notation Eq. (25), we rewrite Eq. (20) in the dimensionless form:

$$\varphi = \sum_\sigma \varphi_\sigma = \sum_\sigma \Bigg\{ -\frac{\delta_\sigma^2}{2}\left(\ln\frac{1}{\delta_\sigma} + \frac{1}{2}\right) + t\int_0^\infty d\xi \ln[f_F(\eta_\sigma + \nu - \sigma b) f_F(\eta_\sigma - \nu + \sigma b)]\Bigg\}, \tag{28}$$

where $t = T/\Delta_0$.

We need to consider the system at fixed doping rather than at fixed chemical potential. Such a choice is better suited for describing usual experimental conditions. To work at fixed x, we should calculate the system's free energy $f = \varphi + \nu x$. To do this, we solve the system of equations (26) at a given doping level x. Then, we calculate φ and f using the obtained values of δ_σ and ν.

In the paramagnetic state, $\delta_\uparrow = \delta_\downarrow = 0$, we readily find from Eqs. (26) and (28) that the chemical potential is proportional to the doping $\nu = x/2$, and

$$\varphi = -\nu^2 - b^2 - \frac{\pi^2 t^2}{3},$$
$$f = \frac{x^2}{4} - b^2 - \frac{\pi^2 t^2}{3}. \tag{29}$$

The properties of the ordered phases will be discussed below.

C. Homogeneous phases at zero temperature

First, let us discuss the homogeneous phases allowed by our mean-field scheme. In what follows, we will limit ourselves to the case $T = 0$.

The task is simplified by the fact that in the mean-field approach, our system becomes "decoupled" and consists of two independent subsystems, labeled by the index σ. The order parameters of these subsystems are mutually independent [see Fig. 1, Eqs. (14) and (16)]. For such a situation, the thermodynamic phases of the system are characterized by a pair of order parameters $(\Delta_\uparrow, \Delta_\downarrow)$.

At zero temperature, we can replace the Fermi functions in the equations above by the Heaviside step function $f_F(\varepsilon) \to \Theta(-\varepsilon)$. After this substitution, the integrations in Eqs. (26)

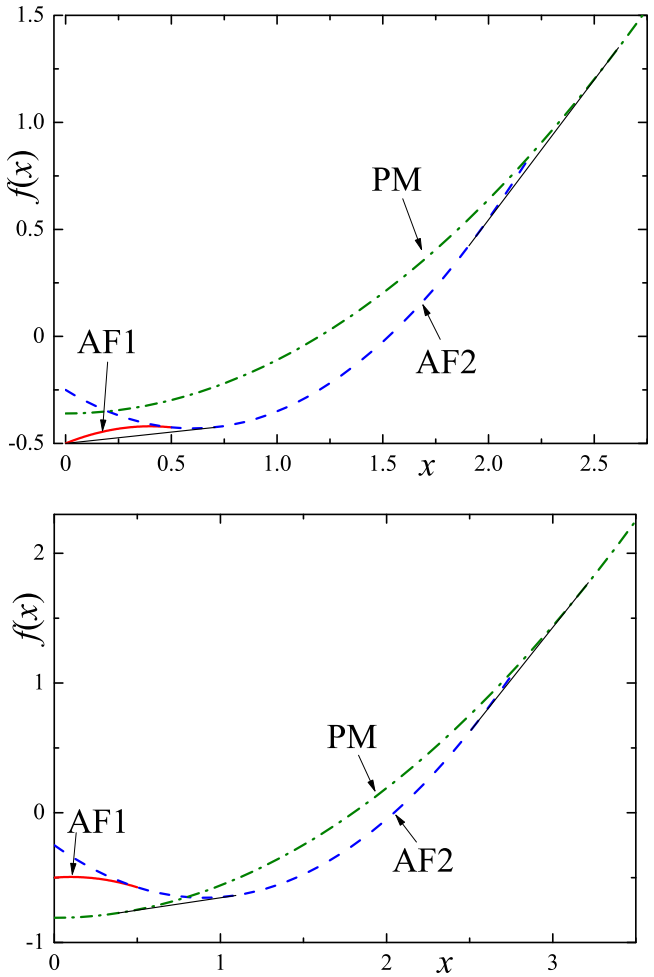

FIG. 2. Dimensionless free energies f for the phases AF1, AF2, and PM (for definition, see the text) vs doping x calculated for $b = 0.6$ (upper panel) and $b = 1.2$ (lower panel). All other homogeneous phases have larger free energies at any doping level. Thin solid (black) lines show the free energies of the phase-separated states found by the Maxwell construction.

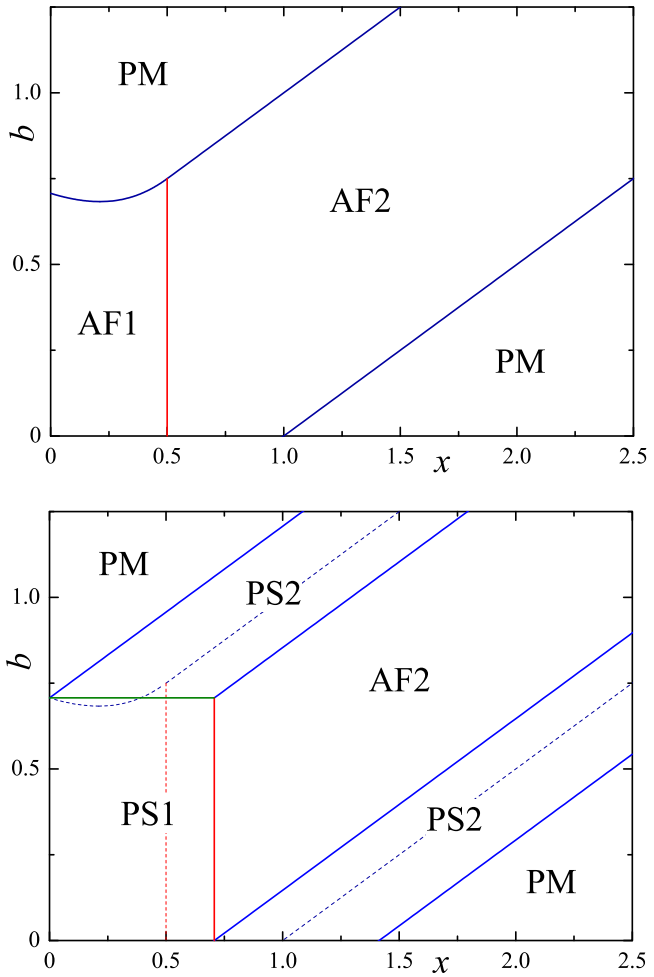

FIG. 3. Phase diagram of the electron model at low fields and zero temperature, calculated neglecting the effect of the Landau quantization. In the upper panel, only homogeneous states are shown. The high-b boundary of the AF1 phase is given by the equation $b = (x + \sqrt{4x^2 - 4x + 2})/2$, while all other boundaries are straight lines. The phase diagram in the lower panel takes into account the possibility of phase separation. Thin dashed curves in the lower panel retrace the phase boundaries from the upper panel. The phase PS1 lies within the boundaries $b < 1/\sqrt{2}$ and $x < 1/\sqrt{2}$. At zero magnetic field the critical doping separating the PS2 and PM phases is equal to $x = \sqrt{2}$. The definitions of homogeneous phases are given in Sec. III C. The phase-separated states are defined in Sec. III D.

and (28) are easily performed and we obtain explicitly

$$\delta_\sigma = \sqrt{2|\nu_\sigma| - 1} = \sqrt{1 - 2|x_\sigma|},$$
$$x_\sigma = -\frac{\partial \varphi_\sigma}{\partial \nu} = \mathrm{sgn}(\nu_\sigma)(1 - |\nu_\sigma|), \quad x = \sum_\sigma x_\sigma, \quad (30)$$
$$\varphi_\sigma = \frac{1}{4} - |\nu_\sigma| + \frac{\nu_\sigma^2}{2},$$

where $\nu_\sigma = \nu - \sigma b$ is a measure of the denesting in subsystem σ. Equations (30) are valid, when $|\nu_\sigma| > \delta_\sigma$ and $\delta_\sigma \neq 0$. This state is metallic with a well-defined Fermi surface and we will refer to it as $\mathrm{AF}_\sigma^{\mathrm{met}}$.

When $|\nu_\sigma| < \delta_\sigma$, we derive from Eqs. (26) and (28) that $\delta_\sigma = 1$, $x_\sigma = 0$, and $\varphi_\sigma = -1/4$. This is an insulating state with the gap in the electron spectrum. We will denote it as $\mathrm{AF}_\sigma^{\mathrm{ins}}$. In the paramagnetic state, $\delta_\sigma = 0$ (further referred to as PM_σ), we obtain $x_\sigma = \nu_\sigma$ and $\varphi_\sigma = -\nu_\sigma^2/2$.

The model is symmetric with respect to the sign of doping and the direction of the magnetic field (up to the replacement $\sigma \to -\sigma$). Consequently, we can consider only the case of electron doping, $x \geqslant 0$, and $b \geqslant 0$.

Thus we have nine possible homogeneous phases: ($\mathrm{AF}_\uparrow^{\mathrm{ins}}$, $\mathrm{AF}_\downarrow^{\mathrm{ins}}$), ($\mathrm{AF}_\uparrow^{\mathrm{met}}$, $\mathrm{AF}_\downarrow^{\mathrm{met}}$), ($\mathrm{PM}_\uparrow$, $\mathrm{PM}_\downarrow$), ($\mathrm{AF}_\sigma^{\mathrm{ins}}$, $\mathrm{AF}_{-\sigma}^{\mathrm{met}}$), ($\mathrm{AF}_\sigma^{\mathrm{ins}}$, $\mathrm{PM}_{-\sigma}$), and ($\mathrm{AF}_\sigma^{\mathrm{met}}$, $\mathrm{PM}_{-\sigma}$), where $\sigma = \uparrow, \downarrow$. We compared the free energies of these phases and found that only three of them can correspond to the ground states of the system ($b > 0$): AF1 = ($\mathrm{AF}_\uparrow^{\mathrm{ins}}$, $\mathrm{AF}_\downarrow^{\mathrm{met}}$), AF2 = ($\mathrm{AF}_\uparrow^{\mathrm{ins}}$, $\mathrm{PM}_\downarrow$), and PM = ($\mathrm{PM}_\uparrow$, $\mathrm{PM}_\downarrow$). The plots of free energies of these phases versus doping x are shown in Fig. 2. The phase diagram in the (x,b) plane for the homogeneous phases is shown in the upper panel of Fig. 3. Note that the phases AF1, AF2, and PM are metallic if $x \neq 0$: one subsystem ($\sigma = \downarrow$) for AF1 and AF2, and both subsystems for the PM phase have a Fermi surface.

D. Phase separation

The phase diagram discussed above was calculated neglecting the possibility of phase separation. However, the shape of the $f(x)$ curves implies such a possibility near the transition lines between the homogeneous states [see solid (black) lines in Fig. 2]. Indeed, the compressibility of the AF1 phase is negative, $\partial^2 f/\partial x^2 < 0$ (see Fig. 2), in the whole doping range where this phase exists. Thus, the homogeneous phase AF1 is unstable, and the separation into the AF1 phase with $x = 0$ and AF2 phase occurs in the system. Let us refer to this phase-separated state as PS1. The range of doping where the phase-separated state is the ground state can be found using the Maxwell construction [55]. The analysis shows that the PS1 phase corresponds to the ground state of the system if $b < b_{c2} = 1/\sqrt{2}$ and $0 < x < 1/\sqrt{2}$.

Other regions of the phase diagram, where an inhomogeneous phase is the ground state, appear in the vicinity of the line separating the AF2 and PM states. The corresponding inhomogeneous phase will be referred to as PS2. The phase PS2 corresponds to the ground state of the system within the doping range $2b + 1/\sqrt{2} < x < 2b + \sqrt{2}$, for any value of b, and also within the range $2b - \sqrt{2} < x < 2b - 1/\sqrt{2}$, if $b > b_{c2}$. The resulting phase diagram of the model is shown in the lower panel of Fig. 3.

IV. ELECTRON–HOLE COUPLING: HIGH MAGNETIC FIELD

For higher magnetic field, we predict the existence of oscillations of the SDW order parameter due to the Landau quantization. This phenomenon is similar to the well known de Haas–van Alphen effect, manifesting itself in the oscillations of the magnetic moment in metals [56]. To outline the general effects and to avoid excessive mathematical difficulties, we restrict our consideration to the case of ideal nesting at zero magnetic field and ideal electron-hole symmetry, that is, $x = 0$ (the grand potential coincides with the free energy), $m_a = m_b = m$, $\Delta g = 0$, $\varepsilon^a_{\max} = \varepsilon^b_{\max} \equiv \varepsilon_{\max}$, and $\varepsilon^a_{\min} = \varepsilon^b_{\min} \equiv \varepsilon_{\min}$.

Using Eqs. (7) and (8), we rewrite the interaction part of Hamiltonian (6) in the form

$$\hat{H}_{\rm int} = \sum_{\sigma\sigma'} \sum_{nmn'm'} \sum_{\mathbf{pp'q}} V_{nmn'm'}(p_x, p_x - q, p'_x, p'_x - q_x) \times \psi^\dagger_{\mathbf{p}na\sigma} \psi_{\mathbf{p'}n'a\sigma} \psi^\dagger_{\mathbf{p'}-\mathbf{q}m'b\sigma'} \psi_{\mathbf{p}-\mathbf{q}mb\sigma'}, \tag{31}$$

where we introduce the matrix elements

$$V_{nmn'm'}(p_x, p_x - q_x, p'_x, p'_x - q_x) = \frac{V}{\mathcal{V}^{2/3} l_B} \int_{-\infty}^{+\infty} d\xi\, \chi_n(\xi - l_B p_x) \chi_m[\xi - l_B(p_x - q_x)] \times \chi_{n'}(\xi - l_B p'_x) \chi_{m'}[\xi - l_B(p'_x - q_x)]. \tag{32}$$

Let us remind that $\mathbf{p}$, $\mathbf{p}'$, and $\mathbf{q}$ in Eq. (31) are 2D momenta having x and z components.

In the mean-field approximation, we apply the following replacement in the interaction Hamiltonian:

$$\begin{aligned} &\psi^\dagger_{\mathbf{p}na\sigma} \psi_{\mathbf{p'}n'a\sigma} \psi^\dagger_{\mathbf{p'}-\mathbf{q}m'b\sigma'} \psi_{\mathbf{p}-\mathbf{q}mb\sigma'} \\ &\quad \to \delta_{\mathbf{q0}} [\eta_{nm\uparrow}(\mathbf{p}) \eta^*_{n'm'\uparrow}(\mathbf{p'}) + \eta_{nm\downarrow}(\mathbf{p}) \eta^*_{n'm'\downarrow}(\mathbf{p'}) \\ &\quad - (\eta_{nm\uparrow}(\mathbf{p}) \psi^\dagger_{\mathbf{p'}m'b\downarrow} \psi_{\mathbf{p'}n'a\uparrow} + \eta_{nm\downarrow}(\mathbf{p}) \psi^\dagger_{\mathbf{p'}m'b\uparrow} \psi_{\mathbf{p'}n'a\downarrow}) \\ &\quad - (\eta^*_{n'm'\uparrow}(\mathbf{p'}) \psi^\dagger_{\mathbf{p}na\uparrow} \psi_{\mathbf{p}mb\downarrow} + \eta^*_{n'm'\downarrow}(\mathbf{p'}) \psi^\dagger_{\mathbf{p}na\downarrow} \psi_{\mathbf{p}mb\uparrow})], \end{aligned} \tag{33}$$

where we assume that mean values $\langle \psi^\dagger_{\mathbf{p}na\sigma} \psi_{\mathbf{p'}mb\bar{\sigma}} \rangle = 0$ if $\mathbf{p} \neq \mathbf{p'}$ and introduce the notation

$$\eta_{nm\sigma}(\mathbf{p}) = \langle \psi^\dagger_{\mathbf{p}na\sigma} \psi_{\mathbf{p}mb\bar{\sigma}} \rangle = \langle \psi^\dagger_{\mathbf{p}mb\bar{\sigma}} \psi_{\mathbf{p}na\sigma} \rangle^*. \tag{34}$$

Substitution (33) makes the total Hamiltonian quadratic in the electron operators. As a result, we are able to calculate the electron spectrum and the grand potential of the system. Minimization of the grand potential with respect to $\eta_{nm\sigma}(\mathbf{p})$ would give us the infinite number of integral equations for the functions $\eta_{nm\sigma}(\mathbf{p})$. This procedure can be substantially simplified if we assume that the functions $\eta_{nm\sigma}(\mathbf{p})$ are independent of the momentum p_x. In other words, we assume here that the electron-electron interactions do not lift the degeneracy of the Landau levels, Eq. (10), with respect to the momentum p_x. Making these assumptions, we effectively restrict the class of variational mean-field wave functions, from which the approximate ground-state wave function is chosen. Without the latter simplifications, the calculations become poorly tractable. Once this approximation is accepted, we obtain the following relation for the mean-field interaction Hamiltonian

$$\hat{H}^{\rm MF}_{\rm int} = \sum_{p_x\sigma} \left[\frac{4\pi \mathcal{V}^{\frac{1}{3}} l_B^2 \Delta_\sigma^2}{V} - \sum_{p_z n} (\Delta_\sigma \psi^\dagger_{\mathbf{p}nb\bar{\sigma}} \psi_{\mathbf{p}na\sigma} + \text{H.c.}) \right], \tag{35}$$

where the SDW order parameters Δ_σ now have the form

$$\Delta_\sigma = \frac{V}{2\pi \mathcal{V}^{1/3} l_B^2} \sum_{p_z n} \eta_{nn\sigma}(p_z). \tag{36}$$

Thus, similar to the case of low magnetic fields considered in the previous section, we have two variational parameters to minimize the grand potential.

We diagonalize the total mean-field Hamiltonian $\hat{H}_e + \hat{H}^{\rm MF}_{\rm int}$ and derive the expression for the grand potential of the system at zero doping (perfect nesting):

$$\Omega = \mathcal{V}^{1/3} \sum_{p_x,\sigma} \left\{ \frac{4\pi l_B^2 \Delta_\sigma^2}{V} - 2T \sum_n \int \frac{dp_z}{2\pi} \ln \left[2\cosh\left(\frac{\sqrt{\Delta_\sigma^2 + \varepsilon_\sigma^2(p_z,n)}}{2T} \right) \right] \right\}, \tag{37}$$

where

$$\varepsilon_\sigma(p_z,n) = \omega_H \left(n + \frac{1}{2} \right) + \frac{p_z^2}{2m} - E_{F\sigma}. \tag{38}$$

In Eq. (37), the summation over n and the integration over p_z are taken within the range determined by the inequalities $\varepsilon_{\min} < \varepsilon_\sigma(p_z,n) < \varepsilon_{\max}$.

The summation over n in Eq. (37) can be replaced by the integration over the 2D momentum $\mathbf{p} = (p_x, p_y)$, when the distance between Landau levels is smaller than the SDW band gap ($\omega_H \ll \Delta_0$). In this case we have

$$n \to \frac{\mathbf{p}^2 l_B^2}{2}, \quad \frac{1}{l_B^2}\sum_n \ldots \to \int d\left(\frac{p^2}{2}\right)\ldots = \int \frac{dp_x dp_y}{2\pi}\ldots.$$

As a result, Eq. (37) is replaced by Eq. (16), where the integration is performed over 3D momentum. This justifies the assumption made in the previous section that we can neglect the effect of the Landau level quantization at low fields.

Minimization of the potential Ω gives the equation for the gap:

$$\frac{1}{4\pi^2 l_B^2}\sum_n \int dp_z \frac{\tanh\left(\sqrt{\Delta_\sigma^2+\varepsilon_\sigma^2(p_z,n)}/2T\right)}{\sqrt{\Delta_\sigma^2+\varepsilon_\sigma^2(p_z,n)}} = \frac{2}{V}. \quad (39)$$

We introduce the density of states

$$\rho_B(E) = \frac{1}{4\pi^2 l_B^2}\sum_n \int dp_z \delta\left[E - \omega_H\left(n+\frac{1}{2}\right) - \frac{p_z^2}{2m}\right], \quad (40)$$

and rewrite Eq. (39) in the form

$$\int_{-E_{F\sigma}}^{\varepsilon_{\max}-E_{F\sigma}} d\varepsilon\, \rho_B(\varepsilon + E_{F\sigma}) \frac{\tanh\left(\sqrt{\Delta_\sigma^2+\varepsilon^2}/2T\right)}{\sqrt{\Delta_\sigma^2+\varepsilon^2}} = \frac{2}{V}. \quad (41)$$

The density of states exhibits equidistant peaks at energies $E = \omega_H(n + 1/2)$. This results in the oscillatory behavior of the order parameters Δ_σ on the magnetic field similar to the de Haas–van Alphen effect [56]. In the limit $\omega_H/\varepsilon_F \ll 1$, one can calculate the density of states analytically. Details of the calculations are presented in Appendix, where for $\rho_B(E)$ we derive expression (A9). Substituting this expression into Eq. (41) at $T = 0$, we obtain

$$\ln\left(\frac{\Delta_\sigma}{\Delta_0}\right) + \sqrt{\frac{\omega_H}{2\varepsilon_F}} \times \sum_{l=1}^{\infty} \frac{(-1)^l}{\sqrt{l}} \cos\left(\frac{2\pi l E_{F\sigma}}{\omega_H} - \frac{\pi}{4}\right) K_0\left(\frac{2\pi l \Delta_\sigma}{\omega_H}\right) = 0, \quad (42)$$

where $K_0(z)$ is the Macdonald function of zeroth order. We solve this equation numerically. Since the Macdonald functions decay exponentially at large values of their arguments, the series in Eq. (42) converges quickly.

The calculated parameters $\Delta_\sigma(B)$ for different g are shown in Fig. 4. We see that both order parameters $\Delta_\sigma(B)$ oscillate when the magnetic field is varied. The amplitudes of the oscillations increase when the ratio Δ_0/ε_F grows (that is, the interaction increases). The oscillations of $\Delta_\uparrow$ and $\Delta_\downarrow$ have the same phases, if g is an integer, and different phases otherwise.

It is seen in Fig. 4 that the order parameters oscillate about some mean value $\widetilde{\Delta}_\sigma$, which is quite robust against the growth of B. This stability, however, is a consequence of the perfect nesting. The value of $\widetilde{\Delta}_\sigma$ decreases with B if we take into account either doping or electron–hole asymmetry. When the doping or asymmetry is high, the SDW order disappears before pronounced oscillations arise.

Note also that the SDW phase is stable at low temperatures since when $T \to 0$ the free energy of the magnetically ordered phase is lower than the PM one. This can be checked directly.

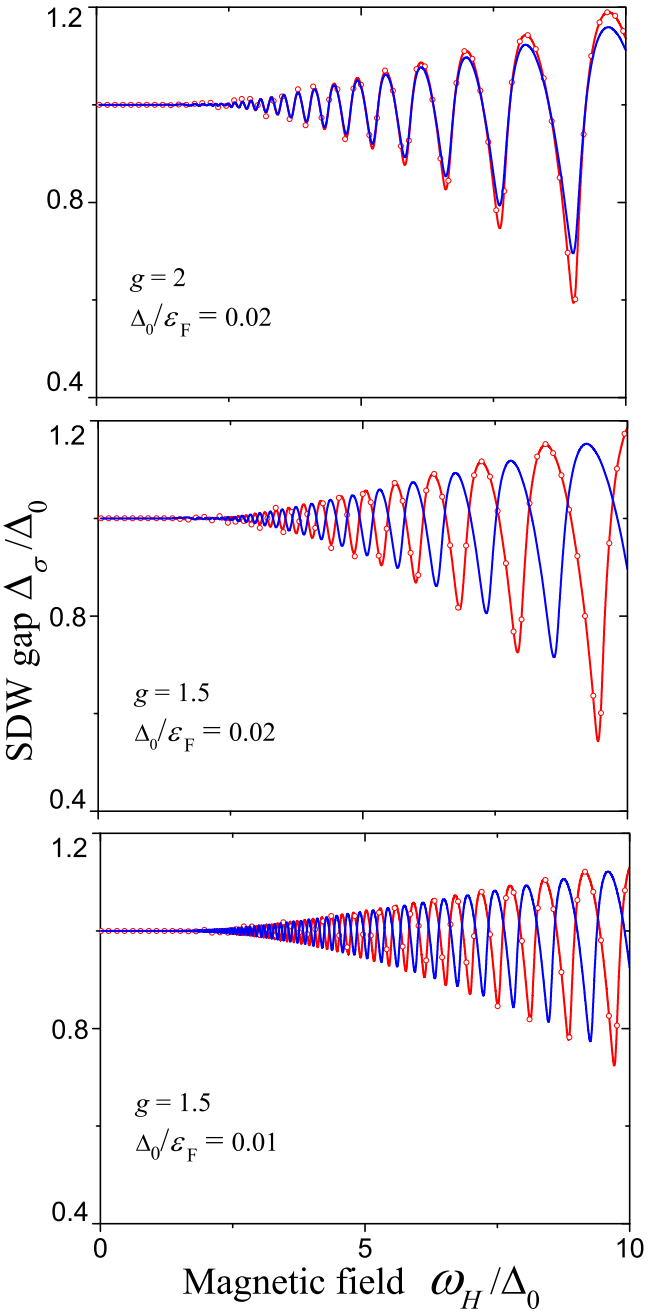

FIG. 4. SDW gaps vs magnetic field calculated at different ratios Δ_0/ε_F and different values of g specified in the plots; $\Delta_\uparrow$ is shown by the (red) solid line with open circles, while $\Delta_\downarrow$ by the (blue) solid line without symbols.

In addition to the behavior of the order parameters, the temperatures of the phase transitions also oscillate as a function of the magnetic field. Note that for $B \neq 0$, there are two transition temperatures, $T_{N\sigma}$, where, as usual, $\sigma = \uparrow, \downarrow$. These temperatures can be calculated using Eq. (41) by taking the limit $\Delta_\sigma \to 0$. This gives the equation

$$\int d\varepsilon\, \rho_B(\varepsilon + E_{F\sigma}) \frac{\tanh(\varepsilon/2T_{N\sigma})}{\varepsilon} = \frac{2}{V}. \quad (43)$$

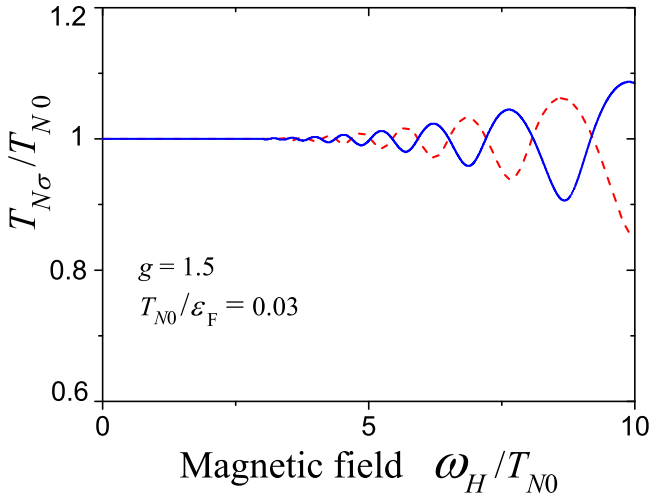

FIG. 5. Dependence of the Néel temperatures on the magnetic field; $T_{N\uparrow}$ is shown by (red) dashed line, while $T_{N\downarrow}$ by (blue) solid one. Parameters are specified in the plot.

Using the density of states (A9), we obtain

$$\ln\frac{T_{N\sigma}}{T_{N0}} = \sqrt{\frac{\omega_H}{2\varepsilon_F}}\sum_{l=1}^{\infty}\frac{(-1)^l}{\sqrt{l}}\cos\left(\frac{2\pi l E_{F\sigma}}{\omega_H}-\frac{\pi}{4}\right) \times \ln\left[\tanh\left(\frac{\pi^2 l T_{N\sigma}}{\omega_H}\right)\right], \quad (44)$$

where T_{N0} is the Néel temperature at zero field, which is related to the SDW gap according to the BCS-like formula $T_{N0} \cong 0.567\Delta_0$. The results of these calculations are shown in Fig. 5.

V. DISCUSSION

In this work, we investigated the effect of an applied magnetic field on weakly correlated electron systems with imperfect nesting. Such study may be relevant for recent experiments on doped rare-earth borides [47]. We found that, when the cyclotron frequency ω_α is comparable to the electron energy gap, Δ_0, the magnetic field effects must be taken into account.

The magnetic field enters the model Hamiltonian via two channels: (i) the Zeeman term, and (ii) orbital (or, diamagnetic) contribution. At low field, $\omega_\alpha < \Delta_0$, and not too small Landé factors g_α, one can neglect the latter contribution and take into account only the Zeeman term. We investigated the combined effects of both terms in the limit of ideal electron-hole symmetry and ideal nesting.

Our study demonstrated that in the presence of the Zeeman term, the number of possible homogeneous magnetically ordered phases significantly increases, compared to the case of $B = 0$. In Sec. III C, we defined as many as nine possible states with different symmetries. If necessary, this list may be increased by taking into account incommensurate SDW phases [13] and phases with "stripes" [23,43]. Of this abundance, only two ordered homogeneous phases could serve as a ground state of our model.

When inhomogeneous states are included into consideration, even the zero-temperature phase diagram becomes quite complex. We would like to remind a reader that, theoretically, the phase separation is a very robust phenomenon. Its generality goes beyond the weak-coupling nesting instabilities of a Fermi surface: the phase separation is found in multiband Hubbard and Hubbard-like models, where the nesting is not crucial [57–61]. It is therefore important to account for its possibility both theoretically, and experimentally.

However, phase separation is not universal: the simplifications of our approach, and the contributions, which we have intentionally omitted (Coulomb interaction, lattice effects, realistic shape of the Fermi surface, disorder, etc), can restore the stability of homogeneous states for a given set of model parameters. For example, the long-range Coulomb repulsion, caused by the charge redistribution in inhomogeneous state, suppresses the phase separation [62–64]. Therefore, in experiments the inhomogeneous states may occupy fairly modest part of the phase diagram, as seen, for example, in Refs. [33,40]. The final location of the segregated region at the phase diagram is affected by the Zeeman energy, as our calculations demonstrated.

The orbital contribution to the Hamiltonian leads to the Landau quantization of the single-particle orbits. As a result, we have demonstrated that both order parameters and the Néel temperatures oscillate as the magnetic field changes. This behavior is associated with the oscillatory part of the single-particle density of states, which emerges due to the Landau quantization. The same oscillations of the density of states are also the cause of the de Haas–van Alphen effect. Yet another related phenomenon, the so-called field-induced SDW, is known to occur in quasi-one-dimensional materials [48–53].

Pronounced oscillations of both Δ_σ and $T_{N\sigma}$ develop at sufficiently large magnetic fields. This circumstance makes their experimental observation a delicate issue. Indeed, the results of Sec. IV were obtained under the assumption of perfect electron-hole symmetry. In a more realistic case, this symmetry is broken, and the magnetic field may cause a transition into a phase with a different order parameter, or destroy the SDW completely before an observable oscillatory trend sets in.

We demonstrated that in electron systems with imperfect nesting the applied magnetic field leads to a significant increase in the number of possible ordered states. It also affects the inhomogeneous, phase-separated states of the system. At higher fields, the Landau quantization causes oscillations of the SDW order parameters and of the corresponding Néel temperatures.

ACKNOWLEDGMENTS

This work is partially supported by the Russian Foundation for Basic Research (Projects No. 14-02-00276 and No. 15-02-02128), Russian Ministry of Education and Science [Grant No. 14.613.21.0019 (RFMEFI61314X0019)], RIKEN iTHES Project, the MURI Center for Dynamic Magneto-Optics via the AFOSR Award No. FA9550-14-1-0040, the IMPACT program of JST, a Grant-in-Aid for Scientific Research (A), and a grant from the John Templeton Foundation.

APPENDIX: DENSITY OF STATES AND THE EQUATION FOR THE GAP

Here, we derive the explicit expression for the density of states given by Eq. (40). The main idea is to divide the density of states into monotonic and oscillatory parts (a similar approach is used, e.g., in Chap. 6 of Ref. [56]). To do this, we first take the integral over p_z in Eq. (40), which gives

$$\rho_B(E) = \frac{1}{4\pi^2 l_B^2}\sqrt{\frac{2m}{\omega_H}}\sum_{n=0}^{N_0}\frac{1}{\sqrt{n+a}}, \tag{A1}$$

where

$$N_0 = \left[\frac{E}{\omega_H} - \frac{1}{2}\right], \quad a = \frac{E}{\omega_H} - \frac{1}{2} - N_0, \tag{A2}$$

and $[\dots]$ denotes the integer part of a real number. The parameter a, by its definition, is the fractional part of $E/\omega_H - 1/2$. Using formulas from the theory of Euler integrals,

$$\frac{1}{\sqrt{x}} = \frac{1}{\sqrt{\pi}}\int_0^\infty \frac{ds}{\sqrt{s}}e^{-xs}, \quad 2\sqrt{x} = \frac{1}{\sqrt{\pi}}\int_0^\infty \frac{ds}{s^{3/2}}(1-e^{-xs}),$$

we write the sum in Eq. (A1) in the form

$$\sum_{n=0}^{N_0}\frac{1}{\sqrt{n+a}} = 2\sqrt{N_0+a} + F(N_0+a) + g(a), \tag{A3}$$

where

$$F(N_0+a) = \frac{1}{\sqrt{\pi}}\int_0^\infty \frac{ds}{\sqrt{s}}\left(\frac{1}{s}+\frac{1}{1-e^s}\right)e^{-(N_0+a)s},$$
$$g(a) = \frac{1}{\sqrt{\pi}}\int_0^\infty \frac{ds}{\sqrt{s}}\left(\frac{e^{-as}}{1-e^{-s}}-\frac{1}{s}\right). \tag{A4}$$

In the limit $\omega_H/\varepsilon_F \ll 1$, one has

$$F(N_0+a) \approx \frac{1}{2\sqrt{N_0+a}} + O\left(\frac{1}{N_0^{3/2}}\right).$$

Substituting all these expressions into Eq. (A1) and expanding it in powers of $\omega_H/\varepsilon_F \ll 1$, we obtain

$$\rho_B(E) \cong \rho_0(E) + \frac{(2m)^{3/2}\sqrt{\omega_H}}{8\pi^2}g[a(E)] + O\left(\frac{\omega_H^2}{\varepsilon_{F\sigma}^2}\right), \tag{A5}$$

where

$$\rho_0(E) = \frac{(2m)^{3/2}\sqrt{E}}{4\pi^2} \tag{A6}$$

is the density of states at zero magnetic field.

The second term in the right-hand side of Eq. (A5) oscillates as B changes, since a is an oscillating function of B, see Eq. (A2). We expand the function $g(a)$ in a Fourier series

$$g(a) = \sum_{l=-\infty}^{+\infty} g_l e^{2i\pi l a}, \quad g_l = \int_0^1 e^{-2i\pi l a}g(a), \tag{A7}$$

where the coefficients of the series can be calculated analytically

$$g_0 = 0, \quad g_l = \frac{1-i\,\mathrm{sgn}(l)}{2}\frac{1}{\sqrt{|l|}} \ (l \neq 0). \tag{A8}$$

Keeping the leading corrections, we can write

$$\rho_B(E) \cong \rho_0(E) + \frac{\rho_0(\varepsilon_F)}{4}\sqrt{\frac{\omega_H}{\varepsilon_F}} \times {\sum_{l=-\infty}^{\infty}}' \frac{1-i\,\mathrm{sgn}(l)}{\sqrt{|l|}}(-1)^l \exp\left(\frac{2i\pi l E}{\omega_H}\right), \tag{A9}$$

where the prime at the summation sign implies that the term with $l = 0$ has to be omitted. Now, we substitute Eqs. (A5)–(A8) in Eq. (39) and obtain the equation for the order parameter in the form

$$\frac{2}{V} = \int_{-E_{F\sigma}}^{\varepsilon_{\max}-E_{F\sigma}} \frac{d\varepsilon}{\sqrt{\Delta_\sigma^2+\varepsilon^2}}\left\{\rho_0(\varepsilon+E_{F\sigma}) + \frac{\rho_0(\varepsilon_F)}{4}\sqrt{\frac{\omega_H}{\varepsilon_F}} \times {\sum_{l=-\infty}^{\infty}}' \frac{1-i\,\mathrm{sgn}(l)}{\sqrt{|l|}}(-1)^l \exp\left(\frac{2i\pi l(\varepsilon+E_{F\sigma})}{\omega_H}\right)\right\}. \tag{A10}$$

As a consistency check, let us consider the limit of vanishing magnetic field. In this case, only the first term in the integral above survives, and one obtains

$$\int_{-E_{F\sigma}}^{\varepsilon_{\max}-E_{F\sigma}} d\varepsilon \frac{\rho_0(\varepsilon+E_{F\sigma})}{\sqrt{\Delta_\sigma^2+\varepsilon^2}} \cong 2\rho_0(\varepsilon_F)\ln\frac{2\sqrt{\varepsilon_F(\varepsilon_{\max}-\varepsilon_F)}}{\Delta_\sigma}. \tag{A11}$$

Thus, at zero magnetic field, we have

$$\frac{1}{V} = \rho_0(\varepsilon_F)\ln\frac{2\sqrt{\varepsilon_F(\varepsilon_{\max}-\varepsilon_F)}}{\Delta_0}. \tag{A12}$$

Assuming that the Fermi level lies near the center of the electron or hole bands ($\varepsilon_F \sim \varepsilon_{\max}/2$), we reproduce Eq. (21) for the Δ_0.

The integration of the second term in Eq. (A10) can be extended over all real values of ε from $-\infty$ to $+\infty$. Taking this integral, we arrive finally to the formula (42) for the gap equation. Equations (44) for the Néel temperatures can be obtained in a similar manner.

[1] D. I. Khomskii, *Basic Aspects of the Quantum Theory of Solids* (Cambridge University Press, Cambridge, 2010).

[2] G. Grüner, The dynamics of charge-density waves, Rev. Mod. Phys. **60**, 1129 (1988).

[3] P. Monceau, Electronic crystals: An experimental overview, Adv. Phys. **60**, 325 (2012).

[4] A. W. Overhauser, Spin density waves in an electron gas, Phys. Rev. **128**, 1437 (1962).

[5] G. Grüner, The dynamics of spin-density waves, Rev. Mod. Phys. **66**, 1 (1994).

[6] J. Ruvalds, C. T. Rieck, S. Tewari, J. Thoma, and A. Virosztek, Nesting mechanism for d-symmetry superconductors, Phys. Rev. B **51**, 3797 (1995).

[7] A. M. Gabovich, A. I. Voitenko, J. F. Annett, and M. Ausloos, Charge- and spin-density-wave superconductors, Supercond. Sci. Technol. **14**, R1 (2001).

[8] K. Terashima, Y. Sekiba, J. H. Bowen, K. Nakayama, T. Kawahara, T. Sato, P. Richard, Y.-M. Xu, L. J. Li, G. H. Cao, Z.-A. Xu, H. Ding, and T. Takahashi, Fermi surface nesting induced strong pairing in iron-based superconductors, Proc. Natl. Acad. Sci. USA **106**, 7330 (2009).

[9] Y.-D. Chuang, A. D. Gromko, D. S. Dessau, T. Kimura, and Y. Tokura, Fermi surface nesting and nanoscale fluctuating charge/orbital ordering in colossal magnetoresistive oxides, Science **292**, 1509 (2001).

[10] A. Shibatani, K. Motizuki, and T. Nagamiya, Spin density wave in chromium and its alloys, Phys. Rev. **177**, 984 (1969).

[11] A. Shibatani, Effect of magnetic field on spin density wave in chromium, J. Phys. Soc. Jpn. **26**, 299 (1969).

[12] A. Shibatani, Néel temperature of the spin density wave in chromium and its alloys, J. Phys. Soc. Jpn. **29**, 93 (1970).

[13] T. M. Rice, Band-structure effects in itinerant antiferromagnetism, Phys. Rev. B **2**, 3619 (1970).

[14] N. I. Kulikov and V. V. Tugushev, Spin-density waves and itinerant antiferromagnetism in metals, Usp. Fiz. Nauk **144**, 643 (1984) [Sov. Phys. Usp. **27**, 954 (1984)].

[15] E. Fawcet, Spin-density-wave antiferromagnetism in chromium, Rev. Mod. Phys. **60**, 209 (1988).

[16] I. Eremin, A. V. Chubukov, Magnetic degeneracy and hidden metallicity of the spin-density-wave state in ferropnictides, Phys. Rev. B **81**, 024511 (2010).

[17] A. Chubukov, Renormalization group analysis of competing orders and the pairing symmetry in Fe-based superconductors, Physica C: Supercond. **469**, 640 (2009).

[18] S. Graser, T. A. Maier, P. J. Hirschfeld, and D. J. Scalapino, Near-degeneracy of several pairing channels in multiorbital models for the Fe pnictides, New J. Phys. **11**, 025016 (2009).

[19] M. G. Vavilov, A. V. Chubukov, and A. B. Vorontsov, Coexistence between superconducting and spin density wave states in iron-based superconductors: Ginzburg-Landau analysis, Supercond. Sci. Technol. **23**, 054011 (2010).

[20] T. Kondo, R. M. Fernandes, R. Khasanov, C. Liu, A. D. Palczewski, N. Ni, M. Shi, A. Bostwick, E. Rotenberg, J. Schmalian, S. L. Bud'ko, P. C. Canfield, and A. Kaminski, Unexpected Fermi-surface nesting in the pnictide parent compounds $BaFe_2As_2$ and $CaFe_2As_2$ revealed by angle-resolved photoemission spectroscopy, Phys. Rev. B **81**, 060507 (2010).

[21] P. M. R. Brydon, J. Schmiedt, and C. Timm, Microscopically derived Ginzburg-Landau theory for magnetic order in the iron pnictides, Phys. Rev. B **84**, 214510 (2011).

[22] J. Schmiedt, P. M. R. Brydon, and C. Timm, Doping dependence of antiferromagnetism in models of the pnictides, Phys. Rev. B **85**, 214425 (2012).

[23] A. A. Gorbatsevich, Yu. V. Kopaev, and I. V. Tokatly, Band theory of phase stratification, Zh. Eksp. Teor. Fiz. **101**, 971 (1992) [Sov. Phys. JETP **74**, 521 (1992)].

[24] A. L. Rakhmanov, A. V. Rozhkov, A. O. Sboychakov, and F. Nori, Phase separation of antiferromagnetic ground states in systems with imperfect nesting, Phys. Rev. B **87**, 075128 (2013).

[25] A. O. Sboychakov, A. V. Rozhkov, K. I. Kugel, A. L. Rakhmanov, and F. Nori, Electronic phase separation in iron pnictides, Phys. Rev. B **88**, 195142 (2013).

[26] A. V. Rozhkov, A. O. Sboychakov, A. L. Rakhmanov, and F. Nori, Electronic properties of graphene-based bilayer systems, Phys. Rep. **648**, 1 (2016).

[27] A. O. Sboychakov, A. V. Rozhkov, A. L. Rakhmanov, and F. Nori, Metal-insulator transition and phase separation in doped AA-stacked graphene bilayer, Phys. Rev. B **87**, 121401(R) (2013).

[28] A. O. Sboychakov, A. V. Rozhkov, A. L. Rakhmanov, and F. Nori, Antiferromagnetic states and phase separation in doped AA-stacked graphene bilayers, Phys. Rev. B **88**, 045409 (2013).

[29] J. T. Park, D. S. Inosov, C. Niedermayer, G. L. Sun, D. Haug, N. B. Christensen, R. Dinnebier, A. V. Boris, A. J. Drew, L. Schulz, T. Shapoval, U. Wolff, V. Neu, X. Yang, C. T. Lin, B. Keimer, and V. Hinkov, Electronic Phase Separation in the Slightly Underdoped Iron Pnictide Superconductor $Ba_{1-x}K_xFe_2As_2$, Phys. Rev. Lett. **102**, 117006 (2009).

[30] D. S. Inosov, A. Leineweber, X. Yang, J. T. Park, N. B. Christensen, R. Dinnebier, G. L. Sun, C. Niedermayer, D. Haug, P. W. Stephens, J. Stahn, O. Khvostikova, C. T. Lin, O. K. Andersen, B. Keimer, and V. Hinkov, Suppression of the structural phase transition and lattice softening in slightly underdoped $Ba_{1-x}K_xFe_2As_2$, with electronic phase separation, Phys. Rev. B **79**, 224503 (2009).

[31] G. Lang, H.-J. Grafe, D. Paar, F. Hammerath, K. Manthey, G. Behr, J. Werner, and B. Büchner, Nanoscale Electronic Order in Iron Pnictides, Phys. Rev. Lett. **104**, 097001 (2010).

[32] T. Goko, A. A. Aczel, E. Baggio-Saitovitch, S. L. Bud'ko, P. C. Canfield, J. P. Carlo, G. F. Chen, P. Dai, A. C. Hamann, W. Z. Hu, H. Kageyama, G. M. Luke, J. L. Luo, B. Nachumi, N. Ni, D. Reznik, D. R. Sanchez-Candela, A. T. Savici, K. J. Sikes, N. L. Wang, C. R. Wiebe, T. J. Williams, T. Yamamoto, W. Yu, and Y. J. Uemura, Superconducting state coexisting with a phase-separated static magnetic order in (Ba, K)Fe_2As_2, (Sr, Na)Fe_2As_2, and $CaFe_2As_2$, Phys. Rev. B **80**, 024508 (2009).

[33] C. Bernhard, C. N. Wang, L. Nuccio, L. Schulz, O. Zaharko, J. Larsen, C. Aristizabal, M. Willis, A. J. Drew, G. D. Varma, T. Wolf, and C. Niedermayer, Muon spin rotation study of magnetism and superconductivity in $Ba(Fe_{1-x}Co_x)_2As_2$ single crystals, Phys. Rev. B **86**, 184509 (2012).

[34] X. Lu, D. W. Tam, C. Zhang, H. Luo, M. Wang, R. Zhang, L. W. Harriger, T. Keller, B. Keimer, L.-P. Regnault, T. A. Maier, and P. Dai, Short-range cluster spin glass near optimal superconductivity in $BaFe_{2-x}Ni_xAs_2$, Phys. Rev. B **90**, 024509 (2014).

[35] E. Civardi, M. Moroni, M. Babij, Z. Bukowski, and P. Carretta, Superconductivity Emerging from an Electronic Phase Separation in the Charge Ordered Phase of $RbFe_2As_2$, Phys. Rev. Lett. **117**, 217001 (2016).

[36] A. Ricci, N. Poccia, G. Campi, B. Joseph, G. Arrighetti, L. Barba, M. Reynolds, M. Burghammer, H. Takeya, Y. Mizuguchi, Y. Takano, M. Colapietro, N. L. Saini, and A. Bianconi, Nanoscale phase separation in the iron chalcogenide superconductor $K_{0.8}Fe_{1.6}Se_2$ as seen via scanning nanofocused x-ray diffraction, Phys. Rev. B **84**, 060511 (2011).

[37] B. Shen, B. Zeng, G. F. Chen, J. B. He, D. M. Wang, H. Yang, and H. H. Wen, Intrinsic percolative superconductivity in $K_xFe_{2-y}Se_2$ single crystals, Europhys. Lett. **96**, 37010 (2011).

[38] A. Ricci, N. Poccia, B. Joseph, D. Innocenti, G. Campi, A. Zozulya, F. Westermeier, A. Schavkan, F. Coneri, A. Bianconi, H. Takeya, Y. Mizuguchi, Y. Takano, T. Mizokawa, M. Sprung, and N. L. Saini, Direct observation of nanoscale interface phase in the superconducting chalcogenide $K_xFe_{2-y}Se_2$ with intrinsic phase separation, Phys. Rev. B **91**, 020503 (2015).

[39] P. Dai, J. Hu, and E. Dagotto, Magnetism and its microscopic origin in iron-based high-temperature superconductors, Nat. Phys. **8**, 709 (2012).

[40] A. Narayanan, A. Kiswandhi, D. Graf, J. Brooks, and P. Chaikin, Coexistence of spin density waves and superconductivity in $(TMTSF)_2PF_6$, Phys. Rev. Lett **112**, 146402 (2014).

[41] G. Campi, A. Bianconi, N. Poccia, G. Bianconi, L. Barba, G. Arrighetti, D. Innocenti, J. Karpinski, N. D. Zhigadlo, S. M. Kazakov, M. Burghammer, M. v. Zimmermann, M. Sprung, and A. Ricci, Inhomogeneity of charge-density-wave order and quenched disorder in a high-T_c superconductor, Nature (London) **525**, 359 (2015).

[42] R. Y. Chen, B. F. Hu, T. Dong, and N. L. Wang, Revealing multiple charge-density-wave orders in $TbTe_3$ by optical conductivity and ultrafast pump-probe experiments, Phys. Rev. B **89**, 075114 (2014).

[43] J. Zaanen and O. Gunnarsson, Charged magnetic domain lines and the magnetism of high-T_c oxides, Phys. Rev. B **40**, 7391 (1989).

[44] R. S. Akzyanov and A. V. Rozhkov, Generation of localized magnetic moments in the charge-density-wave state, Eur. Phys. J. B **88**, 196 (2015).

[45] P. A. Igoshev, M. A. Timirgazin, V. F. Gilmutdinov, A. K. Arzhnikov, and V. Yu. Irkhin, Spiral magnetism in the single-band Hubbard model: The Hartree–Fock and slave-boson approaches, J. Phys.: Condens. Matter **27**, 446002 (2015).

[46] P. A. Igoshev, M. A. Timirgazin, V. F. Gilmutdinov, A. K. Arzhnikov, and V. Yu. Irkhin, Correlation effects and non-collinear magnetism in the doped Hubbard model, J. Magn. Magn. Mater. **383**, 2 (2015).

[47] N. E. Sluchanko, A. L. Khoroshilov, M. A. Anisimov, A. N. Azarevich, A. V. Bogach, V. V. Glushkov, S. V. Demishev, V. N. Krasnorussky, N. A. Samarin, N. Yu. Shitsevalova, V. B. Filippov, A. V. Levchenko, G. Pristas, S. Gabani, and K. Flachbart, Charge transport in $Ho_xLu_{1-x}B_{12}$: Separating positive and negative magnetoresistance in metals with magnetic ions, Phys. Rev. B **91**, 235104 (2015).

[48] L. P. Gorkov and A. G. Lebed, On the stability of the quasi-one-dimensional metallic phase in magnetic fields against the spin density wave formation, J. Physique Lett. **45**, 433 (1984).

[49] A. G. Lebed', Phase diagram of layered quasi-one-dimensional conductors in a magnetic field, Zh. Eksp. Teor. Fiz. **89**, 1034 (1985) [Sov. Phys. JETP **62**, 595 (1985)].

[50] V. M. Yakovenko, Theory of magnetic-field-induced phase transitions in quasi-one-dimensional conductors, Zh. Eksp. Teor. Fiz. **93**, 627 (1987) [Sov. Phys. JETP **66**, 355 (1987)].

[51] G. Montambaux, M. J. Naughton, R. V. Chamberlin, X. Yan, P. M. Chaikin, and M. Ya. Azbel, Phase boundary and magnetization in field-induced spin-density-wave systems, Phys. Rev. B **39**, 885 (1989).

[52] A. Lebed, Field-induced spin-density waves and dimensional crossovers, in *The Physics of Organic Superconductors and Conductors*, edited by A. Lebed (Springer, Berlin, Heidelberg, 2008), pp. 25–40.

[53] A. V. Kornilov and V. M. Pudalov, Magnetic field-induced spin-density wave and spin-density wave phases in $(TMTSF)_2PF_6$, in *The Physics of Organic Superconductors and Conductors*, edited by A. Lebed (Springer, Berlin, Heidelberg, 2008), pp. 487–527.

[54] K. Yamasaki, Spin density wave in magnetic field, J. Phys. Soc. Jpn. **23**, 1209 (1967).

[55] L. D. Landau and E. M. Lifshitz, *Statistical Physics* (Pergamon, Oxford, 1980), Part I.

[56] E. M. Lifshitz and L. P. Pitaevskii, *Statistical Physics* (Pergamon, Oxford, 1980), Part II.

[57] M. J. Calderón, G. León, B. Valenzuela, and E. Bascones, Magnetic interactions in iron superconductors studied with a five-orbital model within the Hartree-Fock and Heisenberg approximations, Phys. Rev. B **86**, 104514 (2012).

[58] Q. Luo, E. Dagotto, Magnetic phase diagram of a five-orbital Hubbard model in the real-space Hartree-Fock approximation varying the electronic density, Phys. Rev. B **89**, 045115 (2014).

[59] K. I. Kugel, A. L. Rakhmanov, and A. O. Sboychakov, Phase Separation in Jahn-Teller Systems with Localized and Itinerant Electrons, Phys. Rev. Lett. **95**, 267210 (2005).

[60] A. O. Sboychakov, K. I. Kugel, and A. L. Rakhmanov, Phase separation in a two-band model for strongly correlated electrons, Phys. Rev. B **76**, 195113 (2007).

[61] A. L. Rakhmanov, A. V. Rozhkov, A. O. Sboychakov, and F. Nori, Phase separation of hydrogen atoms adsorbed on graphene and the smoothness of the graphene-graphane interface, Phys. Rev. B **85**, 035408 (2012).

[62] J. Lorenzana, C. Castellani, and C. Di Castro, Phase separation frustrated by the long-range Coulomb interaction, I. Theory, Phys. Rev. B **64**, 235127 (2001).

[63] J. Lorenzana, C. Castellani, and C. Di Castro, Phase separation frustrated by the long-range Coulomb interaction. II. Applications, Phys. Rev. B **64**, 235128 (2001).

[64] A. Bianconi, N. Poccia, A. O. Sboychakov, A. L. Rakhmanov, and K. I. Kugel, Intrinsic arrested nanoscale phase separation near a topological Lifshitz transition in strongly correlated two-band metals, Supercond. Sci. Technol. **28**, 024005 (2005).